Drug Design, Development and Therapy

Dovepress
open access to scientific and medical research

Open Access Full Text Article

ORIGINAL RESEARCH

Identification of cholest-4-ene-3,6-dione as a Novel Neuroprotectant in Ischemic Stroke and Its Lipidomics

Xiaoshuai Ren[1,*], Feng Lin[2,*], Chaogang Tang[2,*], Yao Liu[3], Guolei Liao[2], Jiabi Liang[3], Wenji Luo[3], Lei Zhang[2], Wenli Chen[3]

[1]Department of Clinical Laboratory, The Fifth Affiliated Hospital of Sun Yat-Sen University, Zhuhai, Guangdong, 519000, People's Republic of China; [2]Department of Cerebrovascular Disease, The Fifth Affiliated Hospital of Sun Yat-Sen University, Zhuhai, Guangdong, 519000, People's Republic of China; [3]Department of Pharmacy, The Fifth Affiliated Hospital of Sun Yat-Sen University, Zhuhai, Guangdong, 519000, People's Republic of China

*These authors contributed equally to this work

Correspondence: Wenli Chen; Lei Zhang, Tel +15626471884; +13726209240, Email chenwenl@mail3.sysu.edu.cn; zhangl92@mail.sysu.edu.cn

Purpose: Stroke is a leading cause of disability and death globally. However, there are few clinical drugs for stroke therapy. Novel and effective neuroprotectants are called on the way.

Methods: In this study, 93 steroids from a constructed steroidal library were randomly numbered and blindly evaluated in an L-glutamate-induced HT-22 oxidative stress model. The neuroprotective effects of 5 candidates were further investigated in potassium deprivation-induced apoptosis of cerebellar granule neurons (CGNs), D-glutamate-induced excitotoxicity of CGNs, and cortical neuron (CN) models.

Results: Interestingly, unblinding revealed that cholest-4-ene-3,6-dione (78), a cholesterol derivative, was first found to have comprehensive neuroprotective effects in all cell models. 78 administration also decreased the infarction volume and improved motor function in middle cerebral artery occlusion (MCAO) model rats. Additionally, 78 treatment decreased intercellular reactive oxygen species (ROS) and NO production in the HT-22 cell model. Finally, lipidomics and molecular docking results showed that 78 may exert its neuroprotective effects by increasing platelet-activating factor (PAF) analog 1-(9Z-pentadecenoyl)-glycero-3-phospho-choline production.

Conclusion: This study indicates that 78, a novel neuroprotectant, is a promising therapeutic candidate with comprehensive neuroprotective effects for the treatment of ischemic stroke by decreasing ROS/reactive nitrogen species (RNS) levels and increasing 1-(9Z-pentadecenoyl)-glycero-3-phospho-choline production.

Keywords: neuroprotection, cholest-4-ene-3,6-dione, anti-ROS, lipidomics, molecular docking

Introduction

Cerebral stroke is an acute cerebrovascular disease with the characteristics of high disability, mortality, and recurrence.[1] Clinically, approximately 75% of strokes are caused by focal cerebral ischemia due to arterial occlusion.[2] The current approaches for ischemic stroke mainly include restoration of blood flow, neuroprotection, and cell replacement therapies throughout the acute recovery progress,[3,4] during which neuroprotection is considered an indispensable treatment.

The pathophysiological mechanisms of ischemic stroke mainly include energy depletion, nerve excitotoxicity, calcium overload, oxidative stress, blood-brain barrier disruption, inflammation, and nerve cell apoptosis,[5] which have been targets for the development of neuroprotectant drugs. However, there are still few neuroprotectants that have been clinically translated. One of the possible reasons for the lack of clinical neuroprotectants is that a single-effect neuroprotectant fails to fully protect against an irreversible cascade of neuronal damage.[6] Therefore, there is an urgent need to investigate novel comprehensive neuroprotectants for the treatment of ischemic stroke.

Received: 11 April 2023
Accepted: 15 November 2023
Published: 11 December 2023

Graphical Abstract

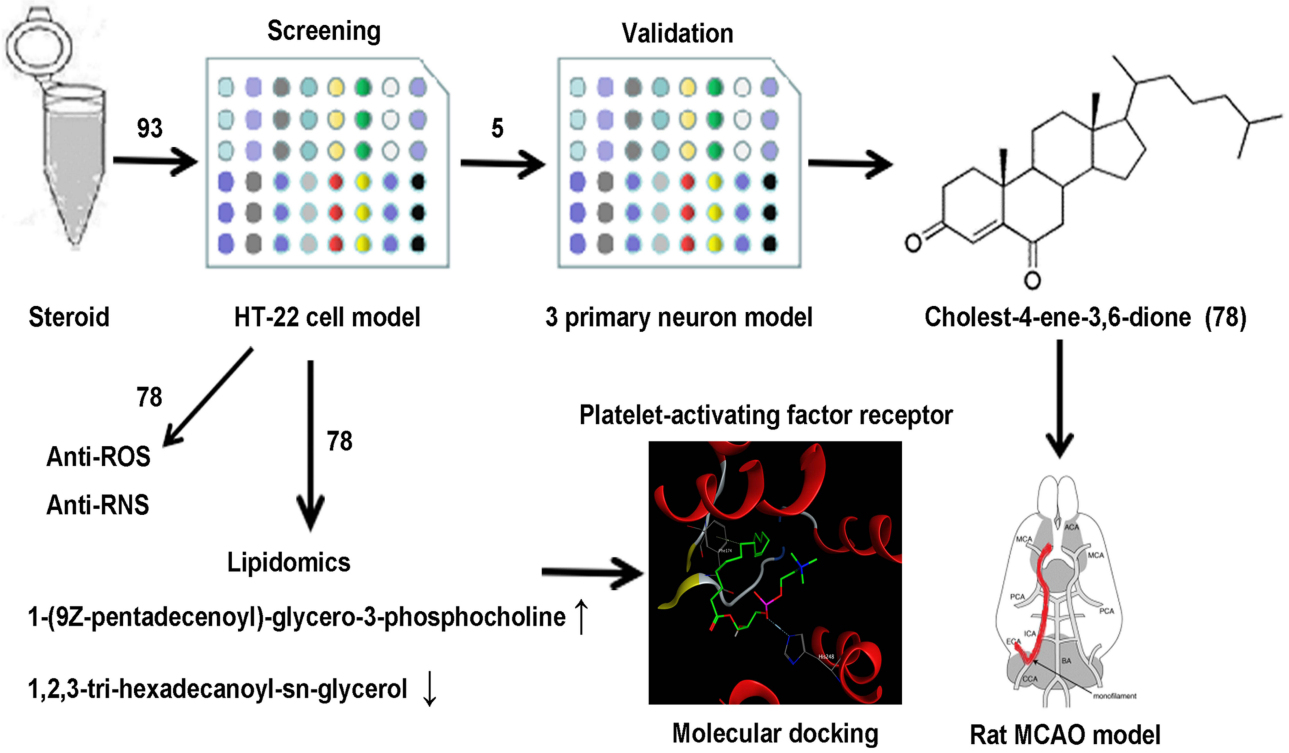

The HT-22 cell line is derived from mouse hippocampal neurons and has morphological and physiological functions similar to those of primary neurons. It is used for the screening of neuroprotectants. Moreover, the L-glutamate (Glu)-induced HT-22 cell death model is a well-recognized model of oxidative stress damage.[7] In addition, the purity of the obtained primary cerebellar granule neurons (CGNs) is high, and they are close to somatic neurons in biological traits. Moreover, potassium is necessary to maintain neuronal depolarization and repolarization. Hence, CGNs treated with 5 mM KCl for 24 h is a commonly used neuronal apoptosis model.[8] Additionally, as an important neurotransmitter, excess glutamate causes neuronal excitotoxicity. D-glutamate-treated CGNs and cortical neuron (CN) death are also considered classical neuronal excitotoxicity models.[9] Finally, middle cerebral artery occlusion (MCAO) is the most widely used cerebral ischemia model at present. Its pathogenesis is similar to that of human ischemic stroke, which gives it great importance in simulating cerebral ischemia and drug screening. An MCAO model constructed using the rat suture embolization method has the following advantages: (1) constant ischemia and reperfusion, simulating different states after human ischemia and thrombolysis; (2) no craniotomy is needed to avoid intracranial infection; and (3) precise control of the occlusion and reperfusion timing. Hence, it is recognized as a standard animal model of focal cerebral ischemia for the evaluation of neuroprotectant activity.

Neurosteroids are important active components of the nervous system that can regulate neuronal excitability through ligand-gated ion channels and some receptors on the cell membrane.[8] As neurosteroids, cholesterol derivatives exert antioxidant, anti-inflammatory, and anti-neurotoxicity effects.[9–11] Moreover, oxidative stress caused by lipid peroxidation is an important factor in neuronal death during ischemic stroke.[12] However, how cholesterol derivatives exert their neuroprotective effects via lipid metabolism detected by lipidomics has rarely been reported.

In this study, 93 steroids were screened using the Glu-HT-22 model. Next, the candidates were further screened in the glutamate-induced cerebellar granular neuron (Glu-CGN), cortical neuron (Glu-CN) excitotoxicity and potassium deprivation-induced cerebellar granular neuron (KD-CGN) primary neuronal injury models. The candidate with the

most comprehensive neuroprotective effects, cholest-4-ene-3,6-dione (78), was chosen for the verification of its neuroprotective activities in a rat MCAO model. The results showed that 78 exerted anti-ROS and anti-RNS effects in Glu-HT-22 model cells. Finally, lipidomics and molecular docking clarified the neuroprotective mechanisms of 78. In conclusion, our research firstly discovered the comprehensive neuroprotective effects of cholest-4-ene-3,6-dione (78) and illustrated its effect of anti-oxidation and lipid regulation. This study provides novel ideas for neuroprotective drugs and targets for the treatment of ischemic stroke.

Materials and Methods

Chemicals

The steroidal library was constructed and synthesized in Professor Jingxia Zhang's library (School of Pharmaceutical Science, Sun Yat-sen University, Guangzhou, PRC) and purchased from commercial resources. All 93 steroids were dissolved in analytically pure dimethyl sulfoxide (DMSO) at a concentration of 10 mM to prepare a stock solution and diluted to 10 μM for a working solution. Other chemical resources are described in the following methods.

Cell Culture

The immortalized hippocampal HT-22 cell line was authenticated by the China Center for Type Culture Collection (Wuhan, China) with a certificate stating the mycoplasma contamination test results were negative for this cell line. Cells were cultured in Dulbecco's Modified Eagle Medium (DMEM, Sigma Aldrich, USA) with 10% fetal bovine serum (FBS, Gibco, USA) and grown on tissue culture plates or dishes in an incubator containing 5% CO_2 at 37°C.

Primary cortical neurons (CNs) were isolated from the cerebral cortexes of newborn Sprague Dawley rats, as previously described.[13] Briefly, whole cerebral cortices were dissected from the brain, washed with Earle's balanced salt solution (EBSS, Gibco, USA) without Ca^{2+} and Mg^{2+}, and then incised to a size of 1 mm3. Following treatment with trypsin (Gibco, USA) and DNase I (Sigma Aldrich, USA), the cells were centrifuged, resuspended, and gently mixed to create a single-cell suspension. Subsequently, the cells were seeded into poly-L-lysine (Sigma Aldrich, USA)-coated plates at a density of $5*10^5$ cells/mL. After 4 h, the medium was completely replaced with serum-free Neurobasal A medium (Gibco, USA) supplemented with 2% B27 (Gibco, USA) and 1% GlutaMAX (Gibco, USA). Ten micromolar cytosine Ara-C (Sigma Aldrich, USA) was added within 24 h. The cortical neurons were cultured for 7 days in a 37 °C containing 5% CO_2 humidified incubator before experiments.

Primary cerebellar granule neurons (CGNs) were isolated from the cerebellum of 7-day-old Sprague Dawley rats, as previously described with minor modifications.[14] Briefly, the whole cerebellum was dissected from the brain, and similar procedures to the CN model procedures were conducted before obtaining a single-cell suspension. Neurons were seeded into poly-L-lysine-coated plates at a density of $4*10^5$ cells/mL. Culture medium contained Basal Medium Eagle (BME, Corning, USA) and 10% FBS, 25 mM KCl (Guangzhou Chemical Reagent Factory, PRC), then the CGNs were cultured for 7 days at 37°C, 5% CO_2 atmosphere before experiments.

MCAO Modelling and Berderson Scoring

The animal experiments were approved by the Ethics Committee of The Fifth Affiliated Hospital of Sun Yat-sen University and performed according to the National Institutes of Health Guide for the Care and Use of Laboratory Animals. Young adult Sprague Dawley rats (225–275 g) were provided from Guangdong Medical Laboratory Animal Center (Guangzhou, China), with free obtain to water and no food for 12 h before surgery. These animals were grouped at random and anesthetized with isoflurane, and their middle cerebral artery was occluded with a nylon monofilament (Southern Medical University, PRC) for 2 h to induce the transient cerebral ischemia, as previously described with minor modifications.[15] After the 2-hour occlusion, different treatments were intraperitoneally performed according to groups and body weight. The rats were placed into a container at 37°C during the entire reperfusion procedure of 24 h. Neurological deficits were evaluated after 24 h of reperfusion with Berderson scoring as previously described.[16] (score 5: animal death; 4: no spontaneous walking; 3: rotating spontaneously toward the left; 2: failure to overcome resistance; 1: the contralateral forepaw buckling to the chest wall in the tail hanging experiment, while the ipsilateral

forepaw extending completely; 0: no visible neurological deficits). Rats with scores of 0 and 4 were excluded in the experiment. Based on the previous evidence,[17] we determined the effect size as 0.6, and calculated a sample size of n=7 with a 2-sided 5% significance level and a power of 80%. Power calculation was done with G*power.

Quantification of Infarct Volume

Infarct volume was assessed with 2,3,5-Triphenyl tetrazolium chloride (TTC; Sigma–Aldrich, USA) staining, as previously described with minor modifications.[18] Briefly, rats were quickly sacrificed under deep anesthesia after reperfusion. The entire brain was isolated and frozen at −20°C for 15 minutes. Coronal sections (2 mm) were obtained from these brain samples and then were stained with 2.0% TTC solution at 37°C for 15 minutes. They were finally immersed into 4% paraformaldehyde solution for 24 h. To avoid the possible interference of brain edema, the infarct volume was corrected by standard methods as follows: corrected infarct volume = contralateral brain volume – (ipsilateral brain volume – infarct volume).

Determination of Intracellular ROS Levels

The oxidation-sensitive probe CM-H2DCFDA (Life, USA) was used to visualize and quantify intracellular ROS levels as previously described with minor modifications.[19] Briefly, cells were seeded in 96-well and 8-well plates, and treatments were performed for 9 h. Cells were stained with 10 μM CM-H2DCFDA and Hoechst 33342 (Beyotime Biotechnology, PRC) in a Hepes-buffered salt solution (HBSS, Amresco, USA) at 37°C for 30 min. Cells in an 8-well plate were photographed with a laser scanning confocal microscope after washing twice with HBSS, and the intensity of fluorescence was quantified by a DYNEX FLUOROLITE 1000 microplate reader (DYNEX Technologies, USA) at an excitation wavelength of 485 nm and emission wavelength of 520 nm, followed by staining with a 10% MTT solution (MP Biomedicals, USA) for 2 h at 490 nm. Cell viability was normalized with and without glutamate, and ROS relative levels = scaled fluorescence intensity/scaled cell viability * 100%.

Determination of NO Levels by ELISA

The quantification of NO production was determined by using ELISA kits (Beyotime Biotechnology, PRC) as previously described.[20] Briefly, the cells were processed with the corresponding reagents, and the supernatant was pipetted into the 96-well plate provided by the ELISA kit to measure NO production at 540 nm. Following MTT (10%) staining for 2 h at 490 nm, NO relative levels = concentration of scaled NO/scaled cell viability * 100%.

Lipidomics Sample Preparation

The lipid extraction method for HT-22 cells was previously described[21] with minor modifications. Cells were washed with DMEM 3 times, and then trypsin was added to the cells for 30s and centrifuged to achieve cell precipitates. After washed with PBS twice, the cells were frozen in liquid nitrogen for 15 minutes, and immediately transferred to a −80°C freezer. The prepared cell samples were delivered to BGI (Shenzhen, PRC) under frozen conditions.

UPLC–MS/MS Analysis and Data Processing

A UPLC system (Waters, UK) coupled with an electrospray ionization (ESI) source was used for nontargeted lipidomics profiling, and the methods used were previously described with minor modifications.[22] For monitoring the performance of the UPLC–MS system, the same volumes of lipid extracts of cells were pooled as quality control (QC) samples. In the validation experiment, an ACQUITY UPLC system (Waters) coupled with a Q-Trap 6500 MS system (AB SCIEX, USA) was used for HPLC/QQQ MRM MS-based pseudotargeted lipid analysis. The detailed methods are described in the Supplementary Material.

For nontargeted lipidomics analysis, the MS data files were pretreated with Progenesis QI software as previously described with minor modifications.[23] Briefly, the filtered data were used to explore the lipid targets. The lipids were identified based on both theoretical fragment and parent mass, and then matched in the Lipid MAPS structure database (LMSD, https://www.lipidmaps.org/). In addition, we further confirmed all of the identifications manually based on the scores.

Molecular Docking

In this experiment, ChemBioDraw Ultra 14.0 software was used to draw the structures of the ligand. The crystal structure of the human platelet-activating factor (PAF) receptor was derived from the Research Collaboratory for Structural Bioinformatics Protein Data Bank (RCSB PDB) with 2.81 Å (PDB code: 5ZKP). We docked proteins and compounds and found the optimal docking configuration for the PAF receptor and compound LMGP01050125 in Molecular Operating Environment (MOE, version 2014.0901) software.

Statistical Analysis

GraphPad Prism 6.0 was used to analyze the experimental data. Quantitative data are presented as the mean ± SEM. The data distribution was analyzed with Normal QQ plot, and homogeneity test was performed by Brown-Forsythe test. Comparisons between the two groups were performed by using a *t*-test method, and multiple groups were compared with one-way ANOVA. Dunnett's multiple comparisons test was utilized alongside ANOVA. The performed tests were also mentioned in figure legends. P values less than 0.05 were considered statistically significant. When sample size per group is less than 5, the bootstrap test was performed to evaluate the confidence interval of statistical quantity by R software 4.0.5, and quantitative data are presented as the median with interquartile range.

Results

Establishing L-Glutamate-Induced HT-22 Injury as a Screening Model

As a result of the advantages of HT-22 cells, a Glu-induced HT-22 cell model was chosen to screen the compounds. Since it was previously reported that concentrations of Glu vary from 1–10 mM,[24,25] 2 mM, 3 mM, and 4 mM concentrations were used to explore the proper concentration of Glu in our research. Our results demonstrated that cell viability significantly decreased with increasing Glu concentration (Figure 1A) after 24 h. The cell viabilities at 2 mM, 3 mM and 4 mM were 62.61(60.91–71.27), 27.81(25.31–46.64), 24.54(11.20–31.12) % (Figure 1B), respectively. A 3 mM concentration of Glu was selected to be used in the screening model. In addition, to explore the HT-22 injury caused by 3 mM Glu within 24 h, the cell viabilities of HT-22 cells treated with Glu for 0 h, 4 h, 8 h, 12 h, 16 h, 20 h, and 24 h were measured. We found that there was a significant difference between the cell viability of the 3 mM Glu group began to be significantly different from that of the control group after 8 h (Figure 1C).

Screening of Drug Candidates in an HT-22 Injury Model

The 93 steroids were randomly numbered, dissolved into DMSO as 10 mM stock solutions, which were diluted to 10 μM to create working solutions. Cell viability (MTT method) and morphology were used as evaluation indicators. The neuroprotective effects of the compounds were evaluated using an Glu-induced HT-22 cell injury model. In the first round of screening, cell viabilities from three wells were used to test for significance. Seven candidates with significant neuroprotective activity compared to that of the Glu group were chosen for the second round of screening. The average of three technical replicates for each candidate was used, and the average of three experiments was used for statistical testing in the second round. The five candidates (round 2), positive control (methylene blue and P7C3), and negative control (36) were selected for the final round of screening with four cell culture experiments (Figure 2A). The cell morphological results showed that compounds 16, 78, and 80 had a significant neuroprotective effect (Figure 2B) similar to the positive control, while compounds 39 and 77 were still protective despite their poor activity. The cell viabilities of 16, 39, 77, 78, and 80 were 63.49(59.20–71.22), 26.74(23.45–31.36), 30.39(24.12–34.18), 56.54(54.09–62.48), 67.00 (60.70–70.76) %, respectively (Figure 2C).

Validation of the Neuroprotective Effect of the Candidates in Cortical Neuron and Cerebellar Injury Models

To further explore the neuroprotection of candidates in primary neuronal injury models, validations were performed in the Glu-CGN, Glu-CN and KD-CGN injury models. We found that 77 and 78 had significant neuroprotective activity (Figure 3A) compared to that of Glu in the Glu-CGN model, with cell viabilities of 73.0±5.4 and 45.9±3.7% compared to

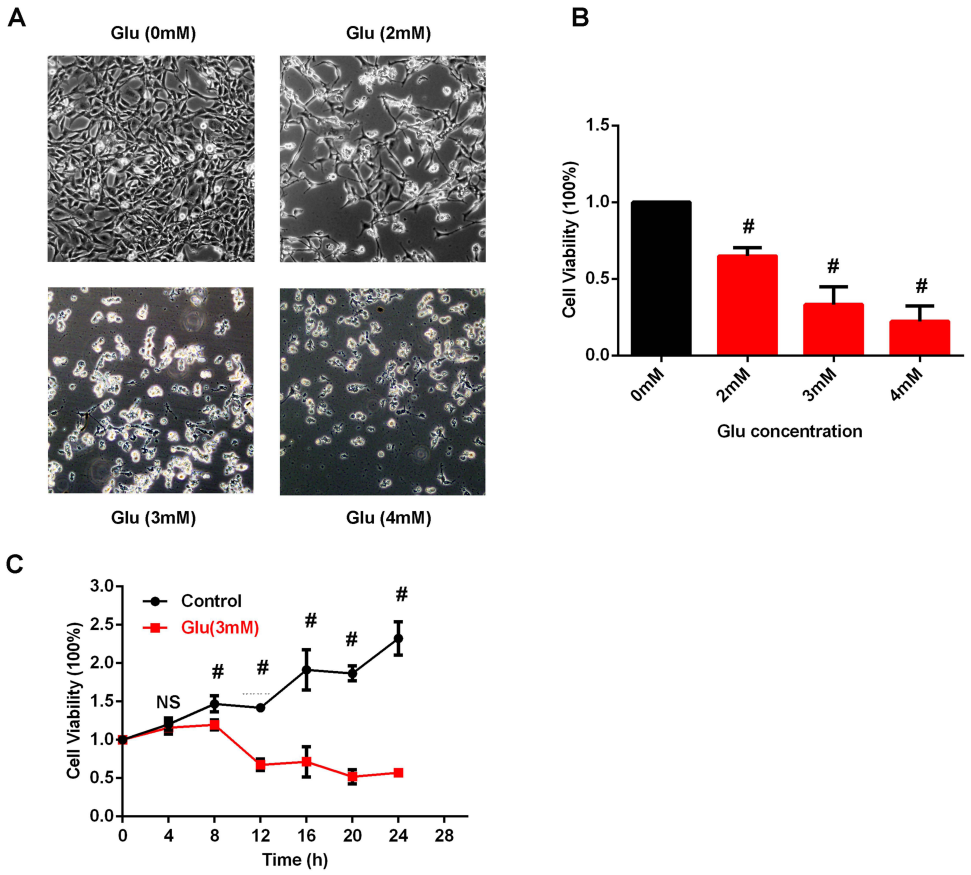

Figure 1 The Glu-induced model is well established with appropriate L-glutamate concentration and time of action. (**A**) Phase-contrast images show the induction of cell death in HT22 cells treated with different concentrations of L-glutamate for 24h (Scale bars, 100 μm). (**B**) HT22 cells were treated with 0,2,3,4 mM L-glutamate, and then cell viability was 62.61(60.91–71.27), 27.81(25.31–46.64), 24.54(11.20–31.12) percent, respectively (median with interquartile range; n = 3 biologically independent samples; bootstrap test). (**C**) HT22 cells viability changes in a time-dependent manner with cells cultured in 3μm L-glutamate (median with interquartile range; n = 3 biologically independent samples; bootstrap test). #There is a statistical difference between the corresponding group and the control group tested by bootstrap test.

24.9±3.2% (Figure 3B). In the KD-CGN model, 16, 77, 78 and 80 had significant neuroprotective activity (Figure 3C) compared to that of the 5K group, with cell viabilities of 65.52(63.44–66.47), 56.82(54.27–57.61), 63.34(61.91–66.05), 64.87(61.85–65.55) percent compared to 42.92(40.59–45.25) percent (Figure 3D). In the Glu-CN model, 16, 39, 78 and 80 had significant neuroprotective activity (Figure 3E) compared to that of the Glu group, with cell viabilities of 69.0 ±2.2, 66.5±3.4, 54.4±4.1 and 86.2±4.7%, respectively, compared to 33.8±2.2% (Figure 3F). Interestingly, we found that 78 had comprehensive neuroprotective effects in each of the cell models (Figure 3G), and unblinding revealed that 78 was cholest-4-ene-3,6-dione (Figure 3H). The anti-apoptotic effect of 78 was further verified by flow cytometry (Figure S1).

Treatment with 78 Attenuates Infarct Volume in the Rat MCAO Model

To validate the neuroprotective activity of 78 in vivo, a rat MCAO model was established. Animals were fasted 24 h before surgery and then subjected to 120 min of ischemia, followed by 24 h of reperfusion after intraperitoneal administration. Finally, they were sacrificed for TTC staining of the brain after Berderson scoring (Figure 4A). The infarction volumes of MCAO, DMSO, MK801, 78 (5 mg/kg), and 78 (10 mg/kg) were 30.2±6.4, 29.8±4.1, 11.8±4.4, 21.3±6.3 and 11.0±2.2%, respectively. Compared with rats treated with DMSO, rats treated with both 78 (5 mg/kg) and 78 (10 mg/kg) had a decreased infarct volume. Moreover, 78 (10mg/kg) had a similar effect in decreasing infarct volume with the positive control MK801 (Figure 4B and C). Rats treated with 78 (10 mg/kg), but not with the lower concentration of 78, exhibited significantly improved motor function compared to that of rats treated with DMSO (Figure 4D).

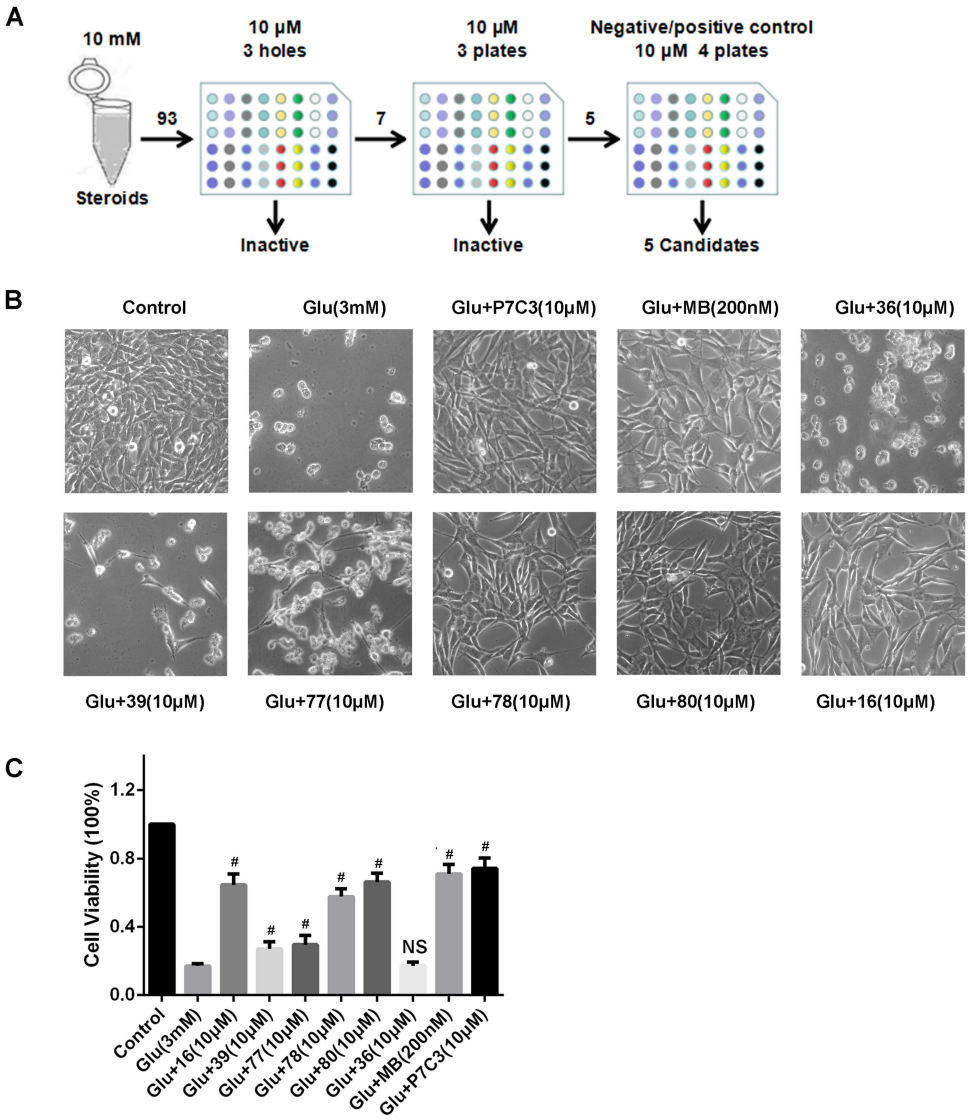

Figure 2 A series of drug candidates are screened for potentially effective agents in HT-22 injury model. (**A**) Flowchart of screening of 93 steroids in HT-22 injury model. (**B**) Cell morphology is observed to exhibit the protective effect of Drug 36, 39, 77, 78, 79, 16 (Scale bars, 100μm). (**C**) The relative cell viability was calculated in the circumstance of 3mM L-glutamate for 24 h (median with interquartile range; n = 4 biologically independent samples; bootstrap test). #There is a statistical difference between the corresponding group and the Glu group tested by bootstrap test.

Treatment with 78 Reduced Intracellular ROS and NO Production

Glutamate-induced HT-22 cell injury is a classical oxidative stress model. Hence, to explore the anti-ROS/RNS effect of 78, the production of intercellular ROS and NO was evaluated in HT-22 cells. We found that glutamate caused a 2.87 ±0.19-fold increase in intracellular ROS levels. Although the anti-ROS activity of 78 (1.42±0.16-fold) was weaker than that of the positive control MB (1.10±0.04-fold), it still significantly reduced intracellular ROS levels when compared to those of each control group (Figures 5A, B and S2). In addition, glutamate caused a 2.95±0.28-fold increase in NO production, and treatment with 78 counteracted the effect of glutamate and significantly reduced NO production by 0.96 ± 0.05-fold (Figure 5C).

Lipidomics and Molecular Docking of 78

According to a previous report,[26] 78 has significant lipid-lowering activity in mice. To investigate whether the neuroprotective mechanism of 78 is correlated with its lipid metabolism, we collected 18 cell samples from control, Glu, and Cholest (Glu+78) groups in the HT-22 model. Then, the lipid internal standards and the total ion

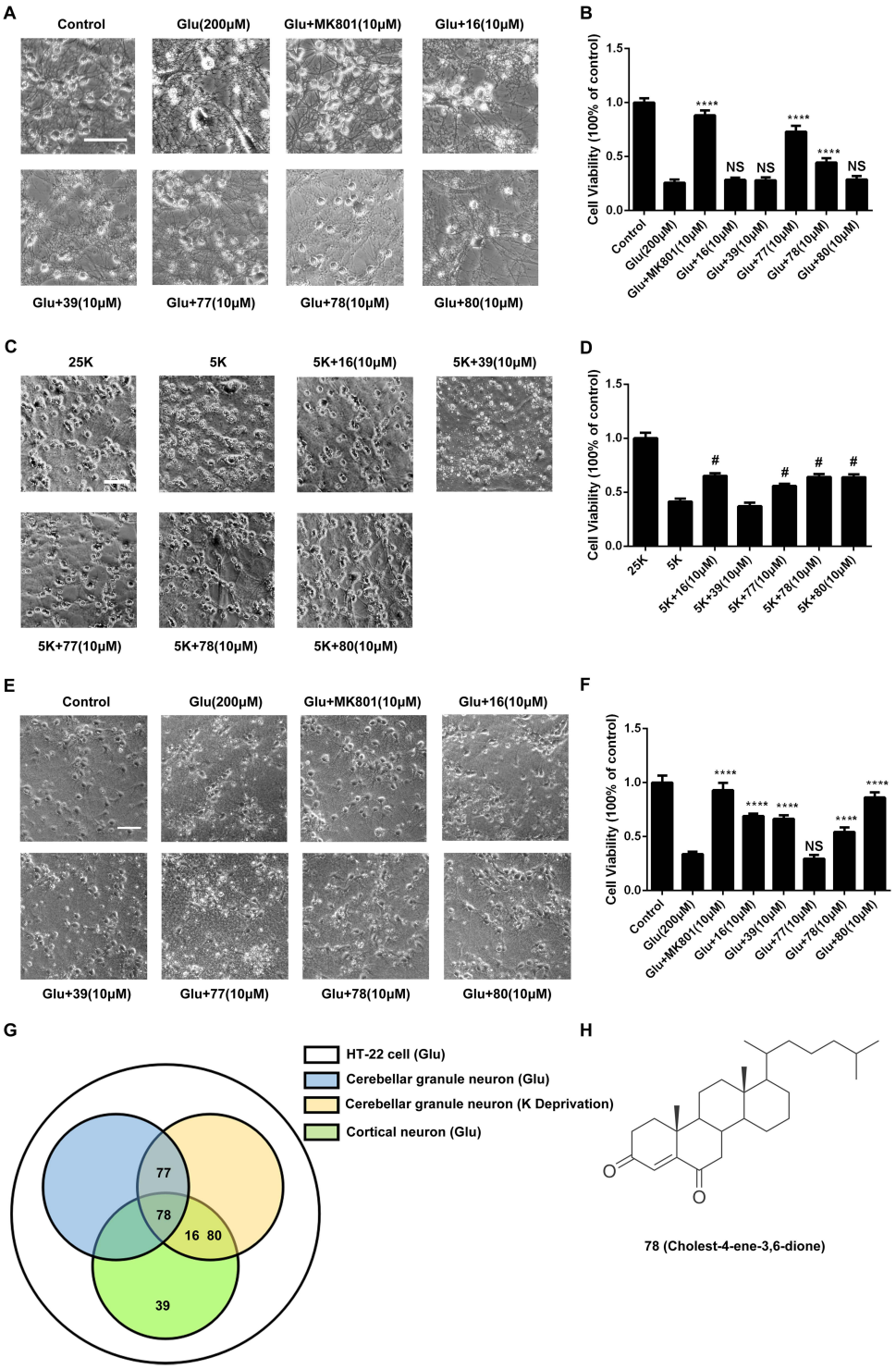

Figure 3 The candidates play a neuroprotective function in cortical neuron and cerebellar injury model. (**A, C** and **E**) Representative images indicate the effect of 5 candidates in glutamate-induced cerebellar granular neuron (Glu-CGN) (**A**)/cortical neuron (Glu-CN) (**C**) excitotoxicity and potassium deprivation-induced cerebellar granular neuron (KD-CGN) apoptosis (**E**) model (Scale bar,100μm). (**B, D** and **F**) Graph of cell viability (expressed as percentage of alive cells) in (Glu-CGN) (**B**) (Dunnett's multiple comparisons test; p= <0.0001,<0.0001,0.9239,0.9480,<0.0001,<0.0001, 0.4978, compared to Glu group relatively)/ (Glu-CN) (**D**) (Bootstrap test; #There is a statistical difference between the corresponding group and the 5K group tested by bootstrap test.)/ (KD-CGN) (**F**) (Dunnett's multiple comparisons test; p=<0.0001, <0.0001,<0.0001,<0.0001,0.5256,<0.0001,<0.0001, compared to Glu group relatively), respectively (mean ± SEM; n = 5 biologically independent samples in B and F, n=3 in (**D**). (**G**) The venn diagram demonstrates that 78 has comprehensive neuroprotective effects in the whole cell models. (**H**) The chemical structural formula of 78. ***p < 0.001, ****p < 0.0001 compared to model group.

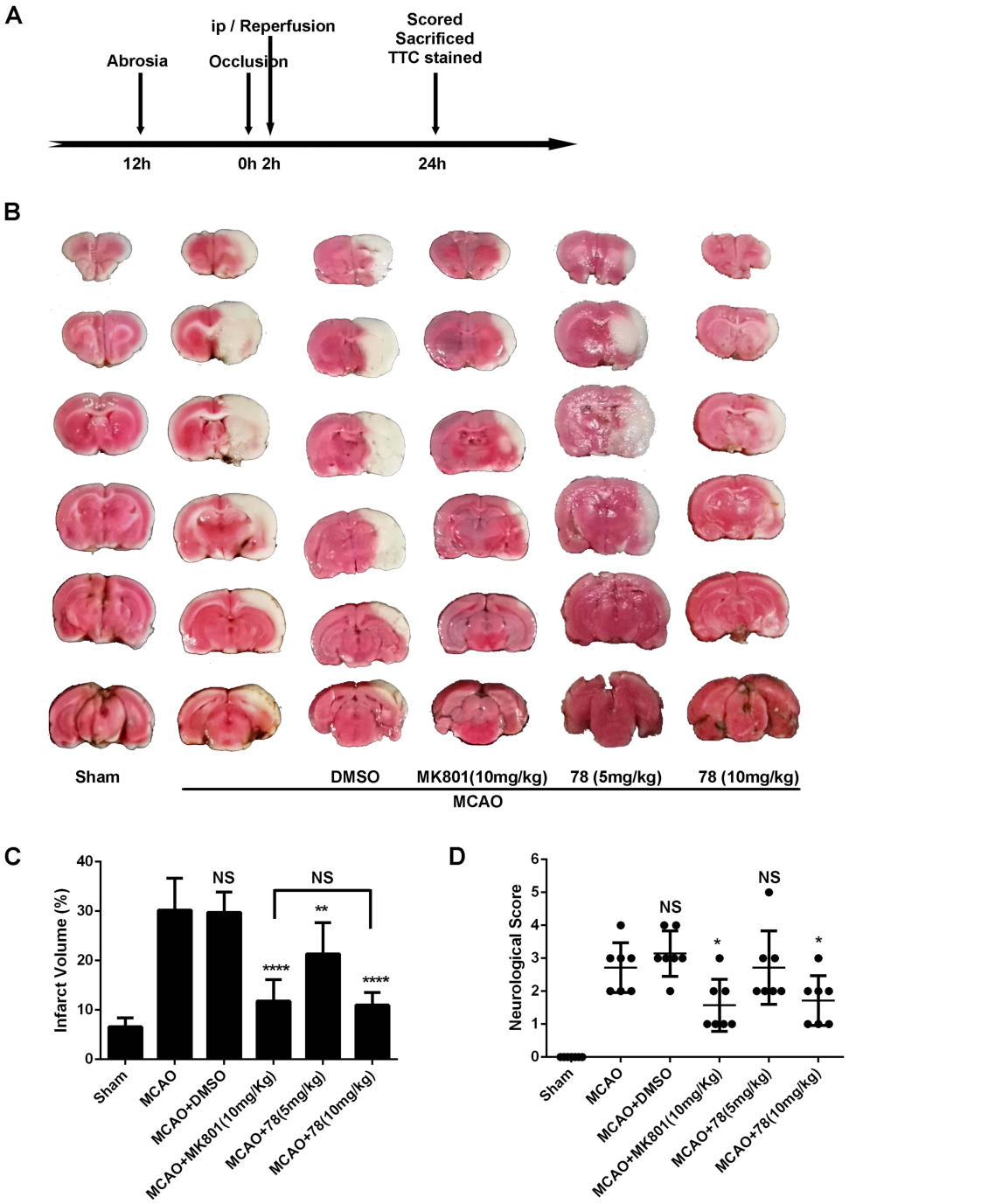

Figure 4 Cholest-4-ene-3,6-dione attenuates infarct volume in rat MCAO model. (**A**) rat MCAO model was performed according to the schedule strictly. (**B**) TTC-stained sections from mice divided into Sham group, tMCAO group with positive drug or DMSO injection, tMCAO group with or without drug injection (n=7 biologically independent samples). (**C** and **D**) Quantification of the infarct volume (**C**) (Dunnett's multiple comparisons test; P=<0.0001,0.9997, <0.0001,0.0056, <0.0001, compared to MCAO group) and neurological deficit score (**D**) (unpaired *t*-test; P=<0.0001,0.2896, 0.0292 for Sham, DMSO, 78(10mg/kg) group compared to MCAO group; Mann Whitney test, P=0.0408,0.8980 for MK801, 78(5mg/kg) group compared to MCAO group) at 24 h after tMCAO. *p < 0.05, **p < 0.001, ****p < 0.0001 compared to tMCAO group.

chromatography (TIC) of QC samples were assessed, and a principal component analysis (PCA) using the QC samples was performed. To identify significant differences between control and Glu and between Cholest and Glu, the following criteria were adopted: VIP>1, fold-change > 1.2 or < 0.8, and Q value < 0.05. 8 and 55 features with significant differences were discovered in control vs Glu and Glu vs Cholest groups respectively. The results indicated that Glu increased TG(16:0/16:0/16:0) levels and decreased LPC(15:1) levels, while Cholest treatment significantly reversed these

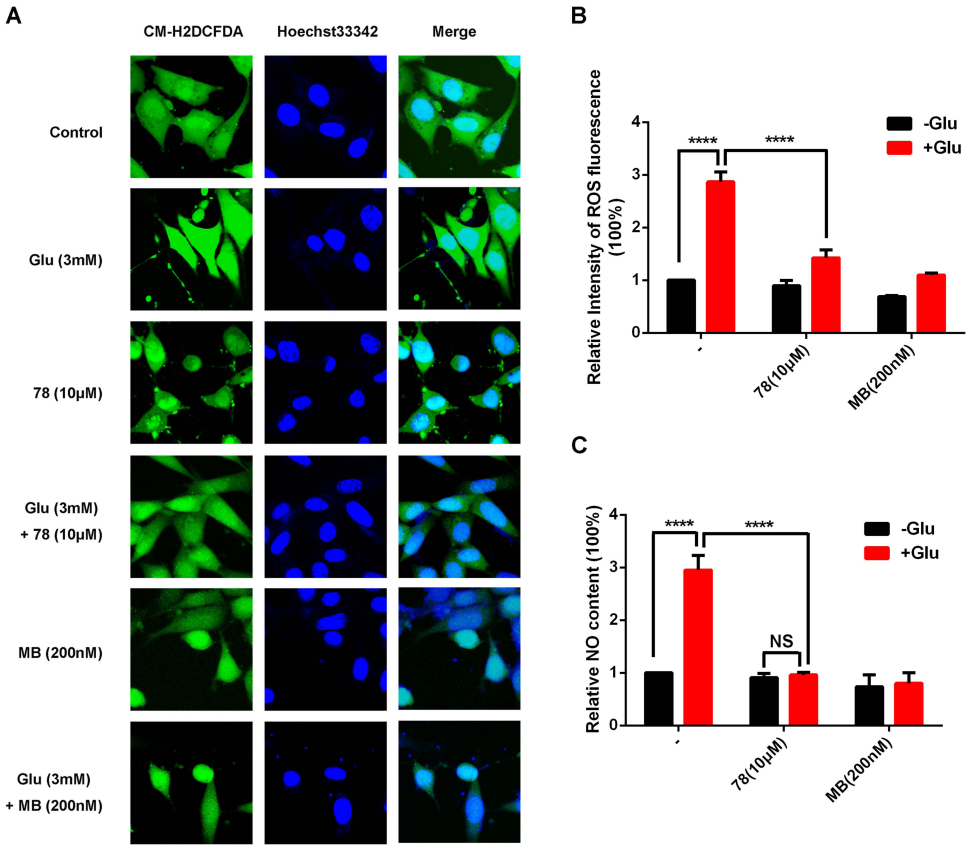

Figure 5 Cholest-4-ene-3,6-dione reduced intracellular ROS and NO production. (**A**) Cells were pretreated with the corresponding drug for 30min. Then cells were treated with or without 3mM L-glutamate for another 9 h. The intracellular ROS formation was monitored using a CM-H2DCFDA probe in a fluorescent microscope. Hoechst 33342 dye was used to stain nuclei. (Scale bar =25 μm). (**B**) Quantification of fluorescence intensity of ROS in HT22 cells (mean ± SEM; n=5 biologically independent samples; Dunnett's multiple comparisons test; P<0.0001 for the other groups compared with Glu group). (**C**) The quantification of NO production was determined by using Elisa Kits. The results are expressed as the percentage of values in the untreated control group (mean ± SEM; n =6 biologically independent samples; Dunnett's multiple comparisons test; P<0.0001 for CON, -Glu+78, +Glu+78 groups compared with Glu group; Dunn's multiple comparisons test, P=0.0013, 0.0299 for -Glu +MB, +Glu+MB groups compared with Glu group). ****P < 0.0001.

changes (Figures 6A and S3). Then, by investigating the LIPID MAPS structural database (LMSD), LPC(15:1) was identified as 1-(9Z-pentadecenoyl)-glycero-3-phosphocholine, and TG (16:0/16:0/16:0) was identified as 1,2,3-tri-hexadecanoyl-sn-glycerol. Furthermore, LPC(15:1) is an analog of PAF, which is a glycerophosphocholine lipid mediator and has been implicated in various pathological processes of the central nervous system.

We conducted Molecular docking studies to better realize the interactions between the PAF receptor and LPC(15:1) or TG (16:0/16:0/16:0). Molecular Operating Environment 2014.0901 was used to dock LMGP01050125 with human platelet-activating factor receptor (PDB code: 5ZKP), and the conformation with the highest binding energy was chosen for further analysis. The binding modes of compound LMGP0105012 in the active site of the human PAF receptor were stabilized by the H-bond interaction with His 248 and H-pi interaction with Phe 174 (Figure 6B). Finally, PAF receptor agonist (PAF) and inhibitor (Ginkgolide B) were used to primary validate the relationship between PAF receptor intervention and neuroprotective effects of 78 in Glu-HT-22 model. The result revealed that 78 demonstrated similar neuroprotective activity to that of Ginkgolide B, and PAF without neuronal toxicity significantly reduced neuroprotective activity 78 (Figure S4), suggesting that 78 and its metabolites may target on PAF receptors.

Discussion

Stroke is a main cause of disability and death globally, and the combination of revascularization and neuroprotection is considered the only effective treatment. Neuroprotectants play an important role in stroke therapy, and our study provides

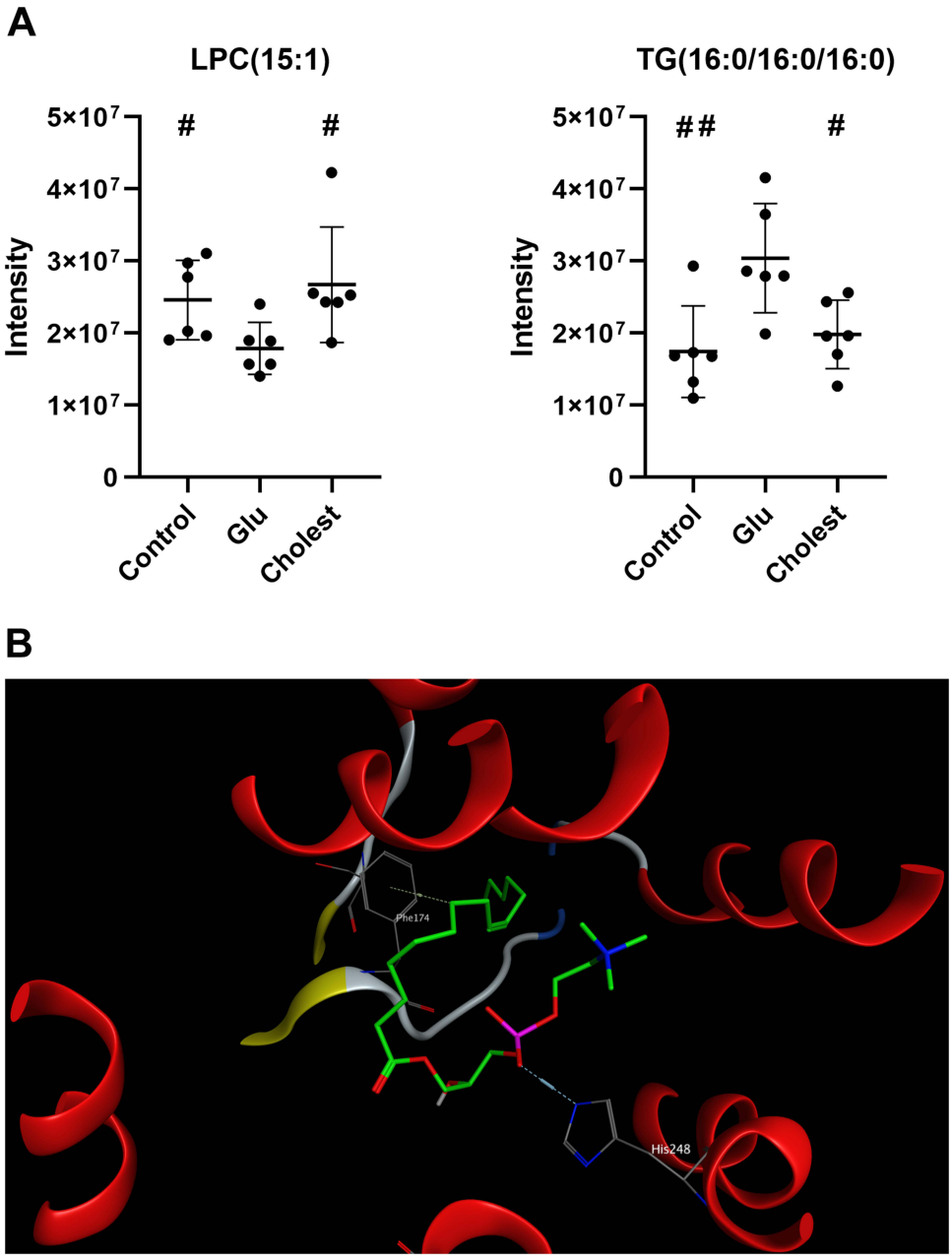

Figure 6 Cholest-4-ene-3,6-dione plays a neuroprotective function possibly via producing a PAF receptor agonist. (**A**) The lipidomics is adopted to identify features with significant differences between control and Glu, Cholest and Glu (VIP>1, fold-change > 1.2 or < 0.8, and Q value < 0.05). Relative signal intensities of TG (16:0/16:0/16:0) and LPC (15:1) changes significantly between GLU and control or Cholest group (mean ± SEM; n =6 biologically independent samples; unpair *t*-test, p=0.0316 between control and Glu group in LPC(15:1); Mann Whitney test, p=0.0152 between Cholest and Glu group in LPC(15:1); unpair *t*-test, p=0.0092,0.0160, compared with Glu group in TG (16:0/16:0/16:0)). $^{\#}P < 0.05$, $^{\#\#}P < 0.01$ compared with GLU group. (**B**) Molecular docking studies were conducted to figure out the interactions between PAF receptor and LPC (15:1) or TG (16:0/16:0/16:0).

a novel neuroprotectant with comprehensive effects in vivo and in vitro, which can conquer cascade injuries in ischemic stroke and indicated its enormous potential for the pharmacological treatment of ischemic stroke.

78 is a steroid with antitumor, antifungal, and antiatherosclerotic properties.[27,28] However, our findings demonstrate, for the first time, its comprehensive neuroprotective activity in cell and animal models. Previous studies revealed that 78 is a main cholesterol derivative found in Rhodiola root extracts, which may partly explain the mechanism by which Rhodiola exerts therapeutic effects on stroke patients.[29] Studies have reported that 78 inhibits pancreatic lipase (PL) and low-density lipoprotein (LDL) oxidation,[29] and it can safely and significantly reduce body weight, abdominal fat, serum

cholesterol levels, and triglyceride levels in mice. This phenomenon further increases the potential of its application for stroke therapy.

Mechanically, the sharp increase in ROS and RNS production leads to the occurrence of oxidative stress, which causes damage to DNA, lipids, and proteins, thus causing neuronal apoptosis and necrosis.[30] Our findings are the first confirmation of the anti-ROS and anti-RNS effects of 78 treatment in an Glu-induced HT-22 oxidative stress model. However, we failed to find changes in the expression of related antioxidant proteins. The anti-oxidative mechanism of 78 needs further investigation.

Previous studies have shown that 78 has favorable lipid-lowering activity.[31] Therefore, lipidomics of 78 was performed using the Glu-HT-22 model to explore its neuroprotective mechanism. Only the levels of 1-(9Z-pentadecenoyl)-glycero-3-phosphocholine, otherwise known as LPC(15:1), and 1,2,3-tri-hexadecanoyl-sn-glycerol were significantly different among the three groups. Interestingly, LPC(15:1) is an analog of PAF, and several PAF receptor antagonists have been reported to alleviate brain damage in animal models of ischemic stroke.[32] Molecular docking showed that LPC(15:1) binds with the PAF receptor, which suggests that 78 attenuates brain injury by increasing the level of LPC(15:1), which antagonizes the PAF receptor. Whether the effect on 1,2,3-tri-hexadecanoyl-sn-glycerol contributes to the neuroprotective activity of 78 needs further investigation.

One limitation of our study was the lack of verification in OGD model. Our initial goal is to screen the multi-target or multi-effect of neuroprotective candidates to treat ischemic stroke. Based on this, anti-oxidative stress, anti-apoptosis and anti-excitotoxicity models were constructed to validate the comprehensive neuroprotective effects of 78. OGD model is a classical ischemic model without representative mechanisms of neuronal injuries. Hence, there was a lack of verification in OGD model in our study. Whether the 78 is neuroprotective in the OGD model needs further investigation. Another limitation of our study was the decision to confirm the candidates quickly. 3 replicates were conducted in cell models, which is not enough to allow for variance analysis. The reason why we did not expand the sample size was partly because there was a statistical difference already.

In conclusion, we firstly find out the comprehensive neuroprotective effect of 78 in cerebral ischemic model, indicating its rosy prospect in treatment. At the same time, we further the PAF receptor as an important neuroprotective target, paving a new road for ischemic stroke treatment.

Conclusion

In summary, our findings identified a promising comprehensive neuroprotectant, 78, which has been verified in several models. It may exert its neuroprotective effects by reducing RNS and ROS levels and increasing 1-(9Z-pentadecenoyl)-glycero-3-phosphocholine production.

Abbreviations

CGNs, cerebellar granule neurons; MCAO, middle cerebral artery occlusion; ROS, reactive oxygen species; PAF, platelet-activating factor; RNS, reactive nitrogen species; Glu, L-glutamate; CN, cortical neuron; DMSO, dimethyl sulfoxide; ESI, electrospray ionization; QC, quality control; LMSD, Lipid MAPS structure database; RCSB PDB, Research Collaboratory for Structural Bioinformatics Protein Data Bank; MOE, Molecular Operating Environment; TIC, total ion chromatography; PCA, principal component analysis; PL, pancreatic lipase; LDL, low-density lipoprotein.

Acknowledgments

We thank Professor Guangmei Yan and Professor Jingxia Zhang (Sun Yat-Sen University) for their devoted technical support. We also appreciate Man Li for professional statistical knowledge.

Author Contributions

All authors made a significant contribution to the work reported, whether that is in the conception, study design, execution, acquisition of data, analysis and interpretation, or in all these areas; took part in drafting, revising or critically reviewing the article; gave final approval of the version to be published; have agreed on the journal to which the article has been submitted; and agree to be accountable for all aspects of the work.

Funding

This research was funded by the National Natural Science Funds of China (82104144 and 81971098), and the Basic and Applied basic Research Fund Project of Guangdong Province (2019A1515110091) to Wenli Chen.

Disclosure

The authors report no conflicts of interest in this work.

References

1. Zhou M, Wang H, Zeng X, et al. Mortality, morbidity, and risk factors in China and its provinces, 1990–2017: a systematic analysis for the Global Burden of Disease Study 2017. *Lancet*. 2019;394(10204):1145–1158. doi:10.1016/s0140-6736(19)30427-1
2. Su Z, Ye Y, Shen C, et al. Pathophysiology of ischemic stroke: noncoding RNA role in oxidative stress. *Oxid Med Cell Longev*. 2022;2022:5815843. doi:10.1155/2022/5815843
3. Liu S, Lin F, Wang J, Pan X, Sun L, Wu W. Polyphenols for the treatment of ischemic stroke: new applications and insights. *Molecules*. 2022;27 (13). doi:10.3390/molecules27134181
4. Tang H, Li Y, Tang W, Zhu J, Parker GC, Zhang JH. Endogenous neural stem cell-induced neurogenesis after ischemic stroke: processes for brain repair and perspectives. *Transl Stroke Res*. 2022. doi:10.1007/s12975-022-01078-5
5. Gu Y, Zhou C, Piao Z, et al. Cerebral edema after ischemic stroke: pathophysiology and underlying mechanisms. *Front Neurosci*. 2022;16:988283. doi:10.3389/fnins.2022.988283
6. Kopach O, Rusakov DA, Sylantyev S. Multi-target action of β-alanine protects cerebellar tissue from ischemic damage. *Cell Death Dis*. 2022;13 (8):747. doi:10.1038/s41419-022-05159-z
7. Sillapachaiyaporn C, Rangsinth P, Nilkhet S, Ung AT, Chuchawankul S, Tencomnao T. Neuroprotective effects against glutamate-induced HT-22 hippocampal cell damage and caenorhabditis elegans lifespan/healthspan enhancing activity of auricularia polytricha mushroom extracts. *Pharmaceuticals*. 2021;14(10):1001. doi:10.3390/ph14101001
8. Zhou MH, Yang G, Jiao S, Hu CL, Mei YA. Cholesterol enhances neuron susceptibility to apoptotic stimuli via cAMP/PKA/CREB-dependent up-regulation of Kv2.1. *J Neurochem*. 2012;120(4):502–514. doi:10.1111/j.1471-4159.2011.07593.x
9. Borozdenko DA, Ezdoglian AA, Shmigol TA, et al. A novel phenylpyrrolidine derivative: synthesis and effect on cognitive functions in rats with experimental ischemic stroke. *Molecules*. 2021;26(20):6124. doi:10.3390/molecules26206124
10. Hu H, Zhou Y, Leng T, et al. The major cholesterol metabolite cholestane-3β,5α,6β-triol functions as an endogenous neuroprotectant. *J Neurosci*. 2014;34(34):11426–11438. doi:10.1523/jneurosci.0344-14.2014
11. Qi J, Ojika M, Sakagami Y. Linckosides A and B, two new neuritogenic steroid glycosides from the Okinawan starfish Linckia laevigata. *Bioorg Med Chem*. 2002;10(6):1961–1966. doi:10.1016/s0968-0896(02)00006-8
12. Wu L, Xiong X, Wu X, et al. Targeting Oxidative Stress and Inflammation to Prevent Ischemia-Reperfusion Injury. *Front Mol Neurosci*. 2020;13:28. doi:10.3389/fnmol.2020.00028
13. Wang B, Huang X, Pan X, et al. Minocycline prevents the depressive-like behavior through inhibiting the release of HMGB1 from microglia and neurons. *Brain Behav Immun*. 2020;88:132–143. doi:10.1016/j.bbi.2020.06.019
14. Blumrich EM, Dringen R. Metformin accelerates glycolytic lactate production in cultured primary cerebellar granule neurons. *Neurochem Res*. 2019;44(1):188–199. doi:10.1007/s11064-017-2346-1
15. Fang Y, Chen X, Tan Q, Zhou H, Xu J, Gu Q. Inhibiting ferroptosis through disrupting the NCOA4-FTH1 interaction: a new mechanism of action. *ACS Cent Sci*. 2021;7(6):980–989. doi:10.1021/acscentsci.0c01592
16. Bieber M, Gronewold J, Scharf AC, et al. Validity and reliability of neurological scores in mice exposed to middle cerebral artery occlusion. *Stroke*. 2019;50(10):2875–2882. doi:10.1161/strokeaha.119.026652
17. Matei N, Camara J, McBride D, et al. Intranasal wnt3a attenuates neuronal apoptosis through Frz1/PIWIL1a/FOXM1 pathway in MCAO rats. *J Neurosci*. 2018;38(30):6787–6801. doi:10.1523/jneurosci.2352-17.2018
18. Zhang B, Zhang HX, Shi ST, et al. Interleukin-11 treatment protected against cerebral ischemia/reperfusion injury. *Biomed Pharmacother*. 2019;115 (17):108816. doi:10.1016/j.biopha.2019.108816
19. Lee DH, Park JS, Lee YS, et al. SQSTM1/p62 activates NFE2L2/NRF2 via ULK1-mediated autophagic KEAP1 degradation and protects mouse liver from lipotoxicity. *Autophagy*. 2020;16(11):1949–1973. doi:10.1080/15548627.2020.1712108
20. Kushairi N, Phan CW, Sabaratnam V, David P, Naidu M. Lion's Mane Mushroom, Hericium erinaceus (Bull.: fr.) Pers. Suppresses H(2)O(2)-induced oxidative damage and LPS-induced inflammation in HT22 hippocampal neurons and BV2 microglia. *Antioxidants*. 2019;8(8):261. doi:10.3390/antiox8080261
21. Sun J, He F, Gao Y, et al. Lipidomics-based study on the neuroprotective effect of geissoschizine methyl ether against oxidative stress-induced cytotoxicity. *J Ethnopharmacol*. 2020;253(20):112636. doi:10.1016/j.jep.2020.112636
22. Liu YN, Hu Y, Wang J, et al. Development of a UPLC-MS/MS method for the determination of orelabrutinib in rat plasma and its application in pharmacokinetics. *Front Pharmacol*. 2022;13:991281. doi:10.3389/fphar.2022.991281
23. Sun R, Gu J, Chang X, et al. Metabonomics study on orthotopic transplantion mice model of colon cancer treated with Astragalus membranaceus-Curcuma wenyujin in different proportions via UPLC-Q-TOF/MS. *J Pharm Biomed Anal*. 2021;193(22):113708. doi:10.1016/j.jpba.2020.113708
24. García-Santos G, Herrera F, Martín V, et al. Antioxidant activity and neuroprotective effects of zolpidem and several synthesis intermediates. *Free Radic Res*. 2004;38(12):1289–1299. doi:10.1080/10715760400017343
25. Tobaben S, Grohm J, Seiler A, Conrad M, Plesnila N, Culmsee C. Bid-mediated mitochondrial damage is a key mechanism in glutamate-induced oxidative stress and AIF-dependent cell death in immortalized HT-22 hippocampal neurons. *Cell Death Differ*. 2011;18(2):282–292. doi:10.1038/cdd.2010.92

26. Chompoo J, Upadhyay A, Gima S, Fukuta M, Tawata S. Antiatherogenic properties of acetone extract of Alpinia zerumbet seeds. *Molecules*. 2012;17(6):6237–6248. doi:10.3390/molecules17066237
27. Lee H, Selvaraj B, Lee JW. Anticancer effects of seaweed-derived bioactive compounds. *Appl Sci*. 2021;11(23):11261. doi:10.3390/app112311261
28. Sali VK, Mani S, Meenaloshani G, Velmurugan Ilavarasi A, Vasanthi HR. Type 5 17-hydroxysteroid dehydrogenase/prostaglandin F synthase (AKR1C3) inhibition and potential anti-proliferative activity of cholest-4-ene-3,6-dione in MCF-7 breast cancer cells. *Steroids*. 2020;159 (27):108638. doi:10.1016/j.steroids.2020.108638
29. Tayade AB, Dhar P, Kumar J, et al. Chemometric profile of root extracts of Rhodiola imbricata Edgew. with hyphenated gas chromatography mass spectrometric technique. *PLoS One*. 2013;8(1):e52797. doi:10.1371/journal.pone.0052797
30. Tuo QZ, Zhang ST, Lei P. Mechanisms of neuronal cell death in ischemic stroke and their therapeutic implications. *Med Res Rev*. 2022;42 (1):259–305. doi:10.1002/med.21817
31. Suzuki K, Shimizu T, Nakata T. The cholesterol metabolite cholest-4-en-3-one and its 3-oxo derivatives suppress body weight gain, body fat accumulation and serum lipid concentration in mice. *Bioorg Med Chem Lett*. 1998;8(16):2133–2138. doi:10.1016/s0960-894x(98)00362-x
32. Zhao B, Fei Y, Zhu J, Yin Q, Fang W, Li Y. PAF receptor inhibition attenuates neuronal pyroptosis in cerebral ischemia/reperfusion injury. *Mol Neurobiol*. 2021;58(12):6520–6539. doi:10.1007/s12035-021-02537-0